High frequency voltage-fed inverter with phase-shift control for induction heating

S.V. Mollov, M. Theodoridis and A.J. Forsyth

Abstract: A voltage-fed resonant LCL inverter with phase-shift control is presented. The control strategy is seen to offer advantages in the megahertz operating region where a constant switching frequency is required. The inverter topology is inherently modular and higher output powers may therefore be readily achieved by adding additional MOSFET switching cells, the devices in each cell having only a modest rating. The inverter steady-state operation is analysed using fundamental frequency analysis. The predictions are verified through time-domain simulations and measurements of a 1.6 MHz 1 kW prototype.

List of Symbols

α	phase shift between pole A and pole B
ϕ	phase between voltage and current in pole A
ψ	phase between voltage and current in pole B
I	current feeding the parallel resonant tank, phasor
i	current feeding the par. resonant tank, instantaneous value
$\boldsymbol{I}_A, \boldsymbol{I}_B$	pole currents, phasors
$\boldsymbol{i}_A, \boldsymbol{i}_B$	pole currents, instantaneous values
L	equivalent work piece inductance
R	equivalent work piece resistance
L_A, L_B	leading-pole and lagging-pole inductances
C	resonant capacitance
$k = L_A/L$	inductor ratio
$Z_0 = \sqrt{L/C}$	characteristic impedance
$Q = Z_0/R$	quality factor of the resonant tank
$\omega_0 = 1/\sqrt{LC}$	angular resonant frequency of the tank
$\omega = 2\pi f$	angular operating frequency
$\omega_n = \omega/\omega_0$	normalised operating frequency
$\boldsymbol{V}_A, \boldsymbol{V}_B$	pole voltages, phasors
v_A, v_B	pole voltages, instantaneous values
V_S	supply voltage

1 Introduction

Industrial applications such as wire and surface heating, plasma generation and dielectric heating require high frequency power supplies that are capable of operating well above 1 MHz at power levels of up to a few tens of kilowatts. Such power supplies normally use a resonant tank to provide predominantly sinusoidal voltages and currents. The resonant tank also provides stored energy for the recharge of the transistor snubber capacitors, thereby enabling low loss soft commutation of the devices, which is essential for megahetz systems.

One of the most common topologies for resonant power supplies is the series resonant converter, Fig. 1*a*. The circuit utilises a simple resonant tank and, when operated slightly above resonance, can offer zero voltage switching (ZVS) for the MOSFETs. Since the maximum device voltage is clamped to the supply voltage, lower voltage MOSFETs with a smaller channel resistance can be used, limiting the conduction losses. The operating frequency can be a significant fraction of a megahertz [1–3]. However, the MOSFETs have to commutate all of the current in the work piece which, in the absence of an impedance matching transformer, can be in the order of kiloamperes.

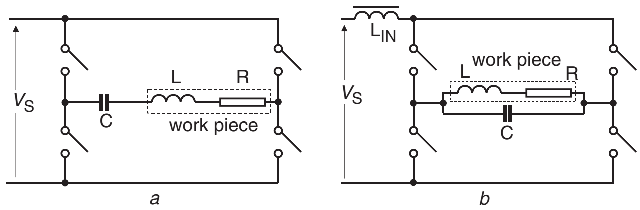

Fig. 1 *Conventional resonant inverters for induction heating*
a Voltage-fed series resonant inverter
b Current-fed parallel resonant inverter

The alternative is to use a parallel resonant tank in a current-fed inverter configuration [4], Fig. 1*b*. The current commutated by the transistors is comparatively small, and the conduction losses are kept under control, but the switches are exposed to the peak resonant voltage which may be much larger than the supply voltage. The problem is exacerbated for applications requiring high-frequency operation, where the quality factor of the parallel resonant tank can be very large. IGBTs are usually employed, as they can block much larger voltages than MOSFETs. However, the maximum operating frequency of these devices is well below that achievable with MOSFETs.

To reduce the switch voltage in the parallel inverter or the switch current in the series inverter, a matching transformer is used to modify the impedance of the work piece, reducing

IEE Proceedings online no. 20031058
doi:10.1049/ip-epa:20031058
Paper first received 6th February 2003 and in revised form 11th September 2003

The authors are with the Electronic, Electrical and Computer Engineering Department, The University of Birmingham, Edgbaston, Birmingham B15 2TT, UK

the device ratings to manageable levels. Alternatively a higher-order resonant tank can be used to perform impedance matching, thereby removing the high-frequency transformer [5–7]. An inverter configuration in which the switch voltage is clamped to the supply voltage (as in the series resonant inverter) and the commutated current is only a fraction of the work piece current (as in the current-fed inverter) is published in [8]. This is achieved by using a parallel resonant tank supplied through an inductor, which matches the impedance of the tank and the impedance that can be handled by the inverter poles. An additional advantage of the circuit is the ability to share the commutated current between a number of inverter poles. The immediate benefit is the capability to use a number of poles to supply a large current to the parallel portion of the resonant tank, yet with benign requirements for the device current and voltage ratings.

The power throughput of resonant inverters is usually regulated either through control of the DC link voltage or by varying the operating frequency. DC link control is undesirable since a dedicated controlled rectifier is required, processing the entire power supplied to the inverter, thereby reducing the overall system efficiency. Furthermore, for operation above 1 MHz, the operating frequency needs to be fixed in order to control pollution from emissions [9, 10]. The legally allowed operating frequency bands are fairly narrow and this precludes the use of variable frequency control.

The fixed frequency, multiple-pole, phase-shift controlled operation of the voltage-fed LCL inverter is now proposed. The inverter operation is explained in the following Section. We then analyse the circuit operation using fundamental frequency analysis. These theoretical predictions are confirmed by time-domain simulations and results from a high-frequency prototype.

2 Inverter Operation

The two-pole LCL inverter is shown in Fig. 2, where the combination of the work piece with the induction coil is represented by an equivalent inductor L and a resistor R. The parallel resonant tank is formed from the parallel combination of the work piece and the resonant capacitor C. The parallel resonant tank is fed by the pole inductors L_A and L_B. The MOSFETs in each pole are driven in anti-phase with duty ratios of almost 50%. A small dead time is included to allow for the ZVS as indicated in the waveforms of Fig. 3. The pole voltages are squarewaves, having an average value of half the supply voltage V_S. This voltage is

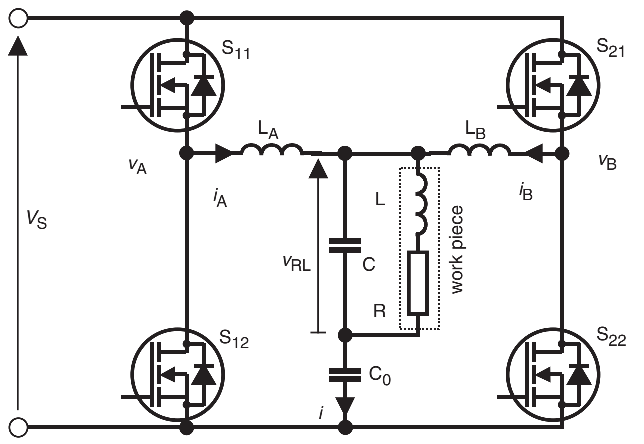

Fig. 2 *Two-pole inverter schematic*

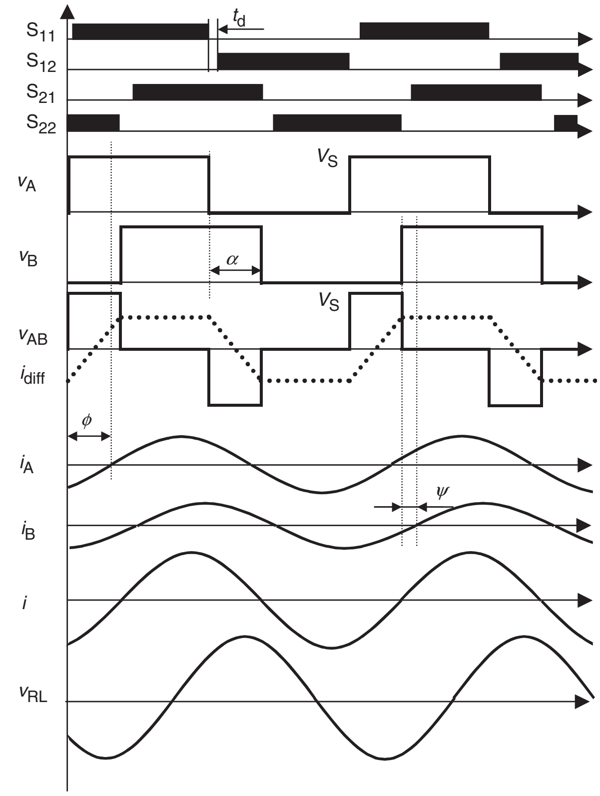

Fig. 3 *Sketched inverter waveforms*

seen across the blocking capacitor C_O, which prevents DC current flowing from the poles through the inductors to ground (Fig. 2).

Power control is executed by phase shifting pole B with respect to pole A by angle α (Fig. 3). The voltage difference v_{AB} between the two poles gives rise to the differential current i_{DIFF}, here shown with a broken line and exaggerated for clarity. This differential current flows from pole A to pole B, but does not contribute to the current i feeding the parallel resonant tank.

Because of the high selectivity of the parallel resonant tank the rest of the waveforms in Fig. 3 are sinusoidal in nature. If the inverter is operated above the resonant frequency of the parallel resonant tank, the leading pole current i_A will be lagging behind the pole voltage v_A by some angle ϕ. The same is true for the lagging pole current i_B and voltage v_B, the respective angle ψ being somewhat smaller for reasons explained later in this Section. The sum i of the two pole currents i_A and i_B feeds the parallel resonant tank, resulting in a large voltage v_{RL} across it. This in turn results in a very large resonant current circulating in the parallel resonant tank and through the work piece.

The lossless ZVS requires that the pole current lags behind the pole voltage. At the instant when a MOSFET turns off, the snubber capacitor C_{sn} across it is being charged by the energy stored in the pole inductor (for this application C_{sn} is simply the body capacitor of the MOSFETs and is therefore not explicitly shown in Fig. 2). The MOSFET therefore is turning off losslessly at zero voltage. The pole voltage swings from one supply rail to the other, and the snubber capacitor of the complementary incoming device is also being discharged by the energy stored in the pole inductor. This process terminates when the pole voltage has fully swung from the one supply rail to the other, at which instant the pole current is diverted from the snubber capacitor to the body diode of the incoming MOSFET. This MOSFET should be turned on very shortly after that, assuring that the transistor is losslessly turned on at zero voltage.

To ensure soft commutation, the energy stored in the pole inductor needs to be sufficiently large to recharge the snubber capacitors. A measure of the available stored energy is the amplitude of the pole current and the phase between the pole's voltage and current. Since i_{DIFF} flows from the leading pole to the lagging pole, its effect is to contribute to the phase shift and current amplitude for the leading pole, but to reduce the phase and the current for the lagging pole. The differential current is therefore seen to assist the soft commutation of the leading pole, but to impede the ZVS of the lagging pole.

3 Fundamental Frequency Analysis

The fundamental frequency equivalent circuit of the converter is shown in Fig. 4. The main assumption is that due to the very high quality factor of the resonant tank, the resonant current in the work piece and the currents through the pole inductors are sinusoidal. The pole output voltages are therefore represented by their fundamental components. Also, the bypass capacitor C_O is assumed to be very large, so the associated resonant frequencies are far below the operating frequencies of interest.

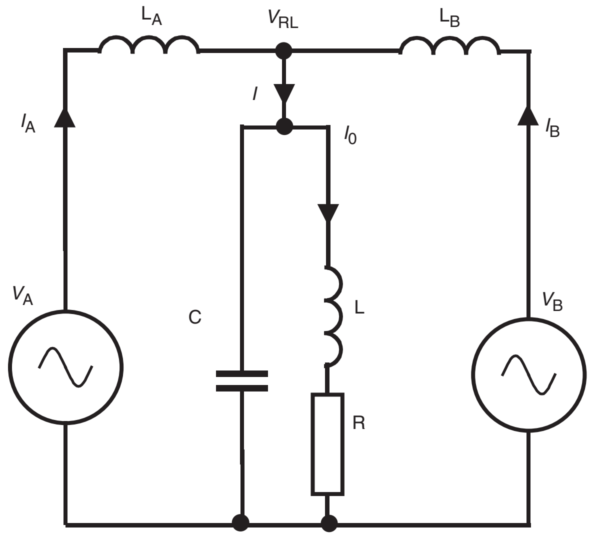

Fig. 4 *Fundamental frequency equivalent circuit*

The parallel tank impedance Z_p is defined as the parallel combination of the impedance of the work piece $R+Z_L$ and the resonant capacitor Z_C:

$$Z_P = \frac{Z_C(R+Z_L)}{Z_C+R+Z_L} \tag{1}$$

The voltage phasor across the work piece, $\boldsymbol{V}_{\mathrm{RL}}$, is:

$$\boldsymbol{V}_{\mathrm{RL}} = Z_P\boldsymbol{I} = Z_p(\boldsymbol{I}_A + \boldsymbol{I}_B) \tag{2}$$

where the phasor $\boldsymbol{I}$ is the vector sum of the pole currents. The pole currents, $\boldsymbol{I}_A$ and $\boldsymbol{I}_B$, are calculated from the voltage imposed across the pole inductors as:

$$\boldsymbol{I}_A = \frac{\boldsymbol{V}_A - \boldsymbol{V}_{\mathrm{RL}}}{\boldsymbol{Z}_{\mathrm{LA}}} \text{ and } \boldsymbol{I}_B = \frac{\boldsymbol{V}_B - \boldsymbol{V}_{\mathrm{RL}}}{\boldsymbol{Z}_{\mathrm{LB}}} \tag{3}$$

where Z_{LA} and Z_{LB} are the impedances of the inductors L_A and L_B respectively.

Substituting (3) into (2) and rearranging will give us the voltage across the work piece as a function of the pole voltages:

$$\begin{gathered}\boldsymbol{V}_{\mathrm{RL}} = \frac{Z_P}{Z_{AB}+2Z_P}(\boldsymbol{V}_A+\boldsymbol{V}_B) \\ \text{where } Z_{AB} = Z_{LA} = Z_{LB} = j\omega L_A\end{gathered} \tag{4}$$

that is, the pole inductors are assumed to have the same values.

The work piece current is:

$$\begin{gathered}\boldsymbol{I}_0 = \frac{\boldsymbol{V}_{\mathrm{RL}}}{R+Z_L} = \frac{Z}{R+Z_L}(\boldsymbol{V}_A+\boldsymbol{V}_B) \\ \text{where } Z = Z_P/(Z_{AB}+2Z_P)\end{gathered} \tag{5}$$

Equation (5) indicates that for a fixed operating frequency the work piece current can be controlled by varying the vector sum of the two pole voltages. This can be achieved either by modulating the DC voltage source, V_S; or by introducing a phase shift between the two poles, which is the approach in this study.

Equations for the pole currents $\boldsymbol{I}_A$ and $\boldsymbol{I}_B$ are obtained by substituting (4) into (3) and rearranging:

$$\begin{aligned}\boldsymbol{I}_A =& \boldsymbol{V}_A\frac{1-Z}{Z_{AB}} - \boldsymbol{V}_B\frac{Z}{Z_{AB}} = \frac{\boldsymbol{V}_A-\boldsymbol{V}_B}{2Z_{AB}} \\ &+ (V_A+V_B)\frac{1-2Z}{2Z_{AB}}\end{aligned} \tag{6a}$$

$$\begin{aligned}\boldsymbol{I}_B =& \boldsymbol{V}_B\frac{1-Z}{Z_{AB}} - \boldsymbol{V}_A\frac{Z}{Z_{AB}} = -\frac{\boldsymbol{V}_A-\boldsymbol{V}_B}{2Z_{AB}} \\ &+ (\boldsymbol{V}_A+\boldsymbol{V}_B)\frac{1-2Z}{2Z_{AB}}\end{aligned} \tag{6b}$$

The first terms in (6*a*) and (6*b*) indicate that there is a differential current, $\boldsymbol{I}_{\mathrm{DIFF}}$, commutated by pole A and pole B, but not contributing to the current flow into the work piece. The work piece current, appearing as a common mode current, is the sum of the second terms of (6*a*) and (6*b*).

3.1 Inverter Steady-state Characteristics

For full power operation, $\alpha=0$, $\boldsymbol{V}_A=\boldsymbol{V}_B$, and the same voltage is applied across the pole inductors. The fundamental frequency equivalent circuit is simplified to the parallel portion of the resonant tank fed through the parallel combination of the pole impedances, that is $Z_{AB}/2$. The impedance presented to the two poles is the same:

$$Z_t = \frac{Z_{AB}}{2} + Z_P = j\frac{\omega L_A}{2} + \frac{j\omega L + R}{j\omega C(j\omega L+R)+1} \tag{7a}$$

This impedance, after substituting with the normalised parameters Z_0, Q and ω_n becomes:

$$Z_t = Z_0\frac{2-k\omega_n^2 + j\omega_n Q(2+k(\omega_n^2+1))}{2Q(1-\omega_n^2)+j2\omega_n} \tag{7b}$$

where $Z_0 = \sqrt{L/C}$ is the characteristic impedance, $Q=Z_0/R$ is the quality factor, $\omega_n = \omega/\omega_0$, $\omega_0 = 1/\sqrt{LC}$ is the normalised operating frequency and k is the ratio between the pole inductance and the work piece inductance.

The magnitude of the impedance Z_t, normalised to Z_0, is shown in Fig. 5. Its evaluation is performed over a range of Q and ω_n chosen in such way that the values are practical and the features of the graph are distinctive.

The total impedance Z_t has a maximum at the load-resonant frequency, largely determined by the resonance of the parallel impedance Z_P. This resonant frequency moves closer to ω_0 as the Q-factor increases. Also, for high Q-factors, the impedance is more sensitive to frequency variations. The value of the impedance Z_t at resonance is

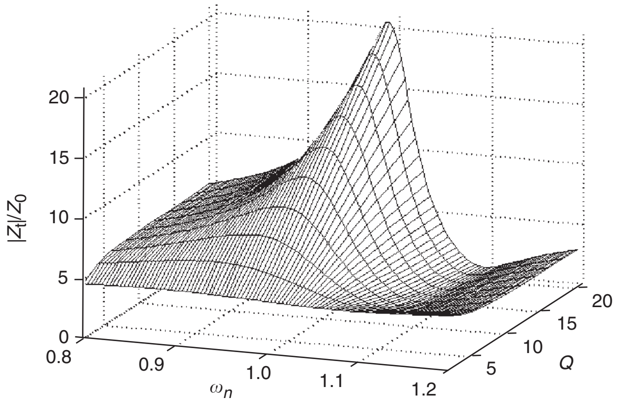

Fig. 5 *Inverter total impedance normalised to Z_0 at zero control angle, $k=10$*

determined mainly by the impedance of the parallel portion of the resonant tank, $Z_P \approx Z_0 Q$ (from (7*b*)), which is much larger than the combined impedance of the pole inductors,

$$\frac{Z_{AB}}{2} = \frac{\omega_0 L_A}{2} = \frac{\omega_0 k L}{2} = \frac{k Z_0}{2}$$

However, as the operating frequency moves further away from resonance, the pole inductor impedance becomes dominant.

The other extreme in the impedance characteristic is a minimum at a second resonant frequency above ω_0. At this frequency Z_p is capacitive and resonates with the parallel combination of the pole inductors. The frequency of this resonance is determined by the parallel combination of Z_p and the combined impedance of the pole inductors. It is calculated by considering the parallel combination of the three inductances (L_A, L_B and L) with the resonant capacitance C and occurs approximately at:

$$\omega_m = \omega_0 \sqrt{\frac{k+2}{k}} \tag{8}$$

It is interesting to note that between the two resonances the impedance can be capacitive and this is more pronounced for high Q-factors. Since the impedance is a minimum in this frequency region, the inverter should be operated slightly above this second resonance, where the phase angle is negative and the impedance plot has a positive gradient, enabling ZVS to be achieved.

The two resonant frequencies, ω_0 and ω_m, are more widely spaced when the inductor ratio k is smaller, according to (8). In practice a large k is needed to achieve sufficiently large current gains (small commutation current for a large work piece current), so the two resonant frequencies are fairly close. The maximum obtainable current gain is calculated by dividing (5) by (6*a*), for $\boldsymbol{V}_A = \boldsymbol{V}_B$ (zero control angle), and substituting with the normalised parameters:

$$\frac{\boldsymbol{I}_0}{\boldsymbol{I}_A} = \frac{2}{1 - \omega_n^2 + j(\omega_n/Q)} \tag{9}$$

and therefore the largest possible current gain equals 2Q for $\omega_n = 1$ and $\alpha = 0$.

The remainder of this Section is concerned with identifying the most desirable operating point of the inverter, for which the current gain is as large as possible while ZVS is maintained for any control angle α.

When the control angle α is different from zero, the differential current will oppose soft commutation of the lagging pole. Equation (6*b*), after substituting with the normalised parameters, is used to find a relation for the angle between voltage and current in the lagging pole in the form:

$$\psi = \arctan \frac{bc - ad}{ac + bd}$$

where

$$\begin{aligned} a &= 1 + \sin(\alpha) Q\omega_n [k(\omega_n^2 - 1) - 1] \\ &\quad + \cos(\alpha)(k\omega_n^2 - 1) \\ b &= Q\omega_n + (1 - k\omega_n^2)(\sin(\alpha) - \cos(\alpha)) \\ c &= \sin(\alpha) k\omega_n (k\omega_n^2 - 2) \\ &\quad + \cos(\alpha) kQ\omega_n^2 [k(\omega_n^2 - 1) + 1] \\ d &= k\omega_n \{\sin(\alpha) Q\omega_n [k(\omega_n^2 - 1) - 1] \\ &\quad - \cos(\alpha)(2 - k\omega_n^2)\} \end{aligned} \tag{10}$$

This angle needs to be negative in order to achieve ZVS over the required control angle range.

In Fig. 6 the entire control range is considered ($\alpha = 0{-}180°$). The plot is generated setting values for k and Q in (10) and solving for the respective normalised frequency for which the angle ψ reaches zero. This value of ω_n is then used to calculate the current ratio ((5) and (6)). In other words, Fig. 6 shows the maximum current ratio achievable for which ZVS is achieved throughout the entire control range.

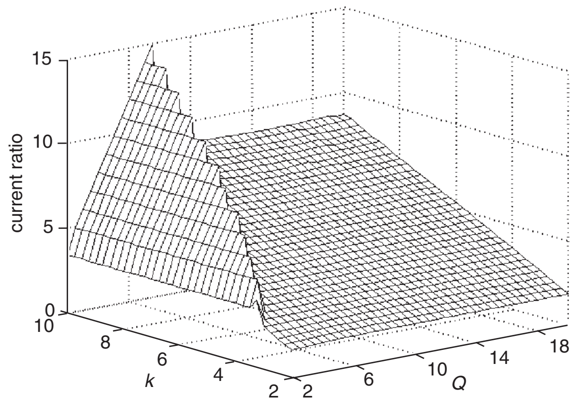

Fig. 6 *Current ratio between the pole current and the load current for ZVS to be maintained throughout the entire control range of α*

There are two distinct regions in the plot, determined by what dominates the total resonant impedance: the pole inductors or the parallel resonant tank. In the right-hand side of the plot (high Q, low k) the current ratios appear to be almost independent of Q, since for given k the current ratio is represented by a horizontal line. On the other hand, for a given Q-factor, a larger inductance ratio results in higher current gains. This region of the plot corresponds to the case when the parallel impedance Z_p is large and dominates the total impedance. Therefore, the operating frequency is a defining factor for soft commutation and should be above the load-resonant frequency.

In the left corner of the plot in Fig. 6, where the values of k are large and Q is comparatively small, the current ratio is independent of k, but rapidly increases with increasing Q-factor. The pole inductors' impedance is large and dominates the total impedance. This ensures that the power factor is lagging for any operating frequency of interest. The maximum current ratio then occurs for $\omega_n = 1$ and equals $2Q$, as could be obtained from (9), by setting $\omega_n = 1$.

The immediate implication is that high inductor ratios are desirable, since they result in the largest current ratios.

However, large pole inductors will increase the total impedance magnitude. This in turn will require a correspondingly higher input voltage which, for practical values of Q, may become prohibitively large.

3.2 Analysis Verification

To verify the theoretical predictions of the fundamental frequency analysis, a series of time-domain simulations was performed, using the SABER [11] package. The resonant components were $L_A = L_B = 10\,\mu$H, $L = 1\,\mu$H, $R = 0.25\,\Omega$ and $55\,\text{m}\Omega$, $C = 158\,$nF, $C_0 = 10\,\mu$F, $f = 2.2\,$MHz resulting in the operating conditions $k = 10$, $\omega_n = 1.1$. Small resistances of $1\,\text{m}\Omega$ were included in series with the reactive components to speed up the convergence of the simulation algorithm. In Fig. 7 the lines denote the theoretical predictions and the stars denote the results from the simulations.

The current ratios are identical for $\alpha = 0$, where we have balanced operation of the two poles. As the control angle α is increased, the current $\boldsymbol{I}_A$ becomes larger than $\boldsymbol{I}_B$, because the differential current phasorially adds to the current of pole A and subtracts from the current commutated by pole B. The same phenomenon explains the variations of the phases between the respective pole voltages and currents. Therefore, the differential current assists the soft commutation of pole A but impedes the ZVS of the lagging pole B and, as is the case shown in Fig. 7 for $Q = 45$, may even cause a leading power factor, where the phase of pole B, ψ, is positive.

There is a very close match between theoretical predictions and simulation data. Deviations become noticeable for large values of the control angle α, where the differential current is comparatively large.

3.3 Multi-pole Inverter Operation

In the more general case, where a larger number of N poles is implemented, the voltage across the parallel portion of the resonant tank is:

$$\boldsymbol{V} = \frac{Z_P}{Z_D + NZ_P} \sum \boldsymbol{V}_{\text{Poles}} \tag{11}$$

where Z_D is the impedance of each pole inductor and $\sum \boldsymbol{V}_{\text{Poles}}$ is the phasor sum of all the pole voltages. Similarly, the load current is:

$$\boldsymbol{I}_0 = \frac{1}{R + Z_L} \frac{Z_P}{Z_D + NZ_P} \sum \boldsymbol{V}_{\text{Poles}} \tag{12}$$

For fixed frequency operation, the impedances are constant and the load current depends only on the phasorial sum of the pole voltages.

Figure 8*a* shows the fundamental frequency equivalent circuit for three poles, $N = 3$. The pole voltages are displaced by an equal phase shift angle, α. Power throughput is controlled by varying the phase between these poles, as shown (in terms of phasors) in Fig. 8*b* for $\alpha = 120°$ and $\alpha = 15°$. The largest power is delivered to the load when the control angle $\alpha = 0°$. Zero power is delivered to the load when the control angle is $\alpha = 360°/N$, here 120°.

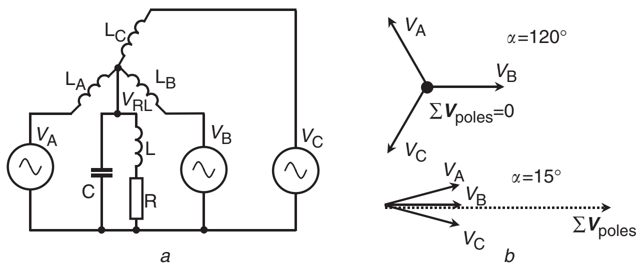

Fig. 8 *Three-pole LCL inverter*
a Fundamental frequency equivalent circuit
b Phasors of the pole voltages and their sum for control angles $\alpha = 120°$ and $\alpha = 15°$

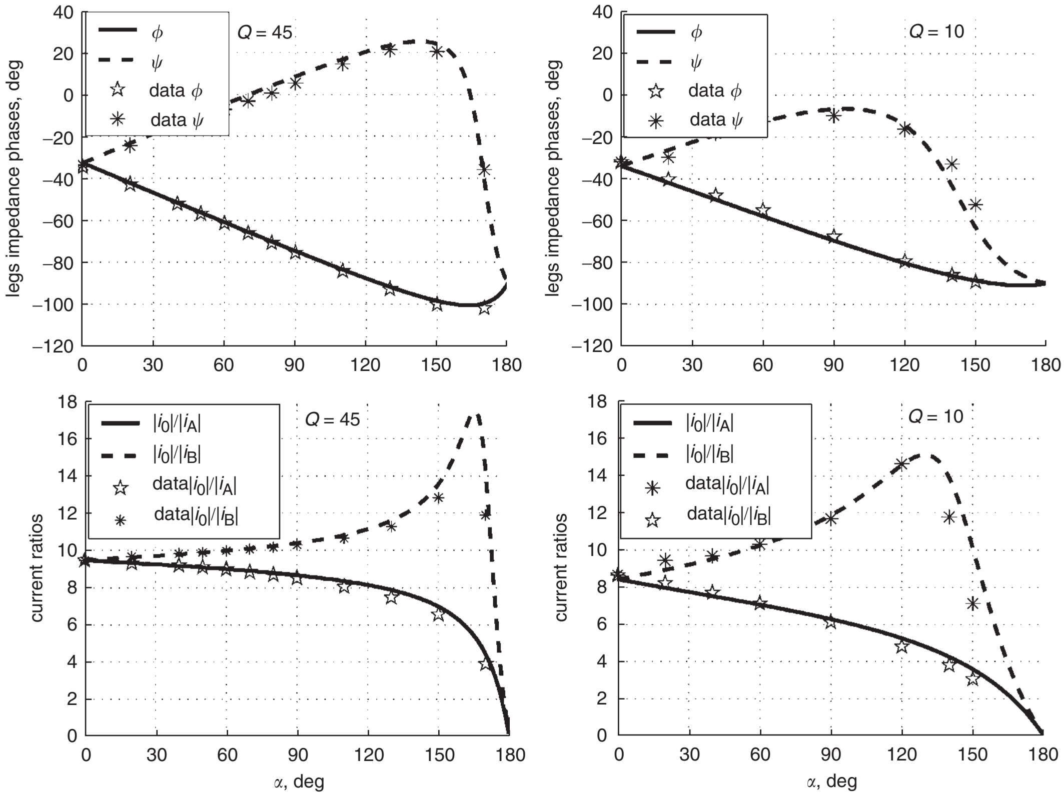

Fig. 7 *Comparison between fundamental frequency model predictions and time-domain simulations; $k = 10$, $\omega_n = 1.1$*

Theoretically, higher harmonics (odd multiples of the fundamental) could conspire to produce a substantial power flow. For example, three legs operating with a phase-shift of $\alpha = 120^\circ$ will result in a zero fundamental voltage across the resonant tank, but the triplen harmonics in each leg voltage will be in phase. However, this will result in very little current flow in practical circuits due to the high selectivity of the parallel resonant tank.

The current commutated by each pole is:

$$\boldsymbol{I}_{\mathrm{N}} = \frac{\boldsymbol{V}_{\mathrm{N}}}{Z_{\mathrm{D}}} - \frac{1}{Z_{\mathrm{D}}} \frac{Z_{\mathrm{p}}}{Z_{\mathrm{D}} + NZ_{\mathrm{P}}} \sum \boldsymbol{V}_{\mathrm{Poles}} \tag{13}$$

If the input voltage and the power throughput of the inverter are to be kept constant, increasing the number of poles means that the value of the pole inductor L_N needs to be NL_0, where L_0 is the pole inductance for the single-pole inverter. Each pole then will commutate a N-times smaller current. This allows small-current, fast-switching devices to be used, enabling efficient high-frequency inverter operation at the expense of a larger number of devices and pole inductors.

4 Prototype Measurements

Equations (6), (9) and (10) were used to construct an inverter with the parameters summarised in Table 1. Table 2 gives the resulting calculated components together with the components that were actually implemented in the prototype.

IRF740LC devices ($R_{on} = 0.5\,\Omega$, $V_{BR} = 400\,\mathrm{V}$, $I_D = 10\,\mathrm{A}$) were used for the MOSFETs since they offer fast switching and have sufficient current and voltage ratings. The pole inductors were air-cored to eliminate the core losses. No other attempt was made to minimise the inverter losses.

Figure 9 shows the measured waveforms for full power. The trace (i) is for the pole B voltage, trace (ii) is the pole B current, trace (iii) is the pole A current and trace (iv) is the current in the resonant tank. ZVS is easily achieved due to the 50° phase between $\boldsymbol{V}_B$ and $\boldsymbol{I}_B$. The switching frequency is 1.6 MHz and the power throughput is 1 kW. The ratio between the commutated current and the load current is in excess of ten.

ZVS conditions are maintained throughout the control range. Figure 10 shows the same waveforms as in Fig. 9, but for a control angle of $\alpha = 144^\circ$. This operating condition is approximately the worst case for ZVS in pole B, since the phase is a minimum and the amplitude of the commutated current is relatively small. The difference between the two pole currents is clearly seen, the lagging current (trace (ii)) having a perceptibly lower amplitude.

The load short-circuit condition is a common fault mode in induction heating applications, particularly problematic

Table 1: Parameters used for the design of the prototype

P_o, W	P_{min}, W	V_S, V	R, mΩ	L, μH	f_{sw}, MHz
1000	0	310	0.235	0.94	1.6

Table 2: Component values from design calculations and values implemented in the prototype

	L, μH	R, mΩ	C, nF	ω_n	L_A, μH	C_0, nF
Calculated	0.94	0.264	12.4	1.08	12.6	200
Implemented	1.07	0.291	10.8	1.06	15	4x470

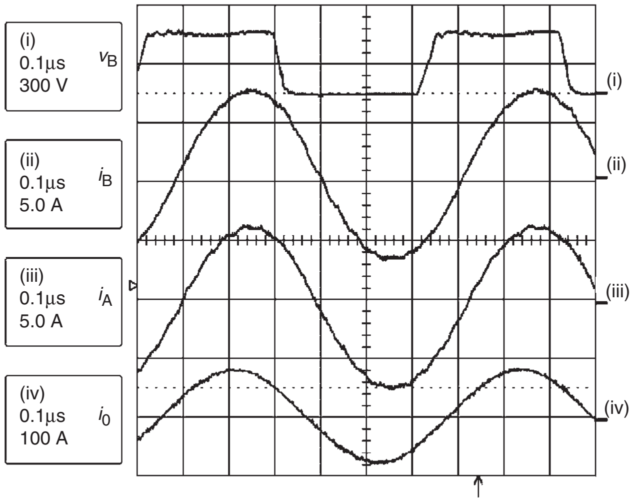

Fig. 9 *Full power throughput prototype measurement*
(i) Lagging pole voltage
(ii) Lagging pole current
(iii) Leading pole current
(iv) Work piece current

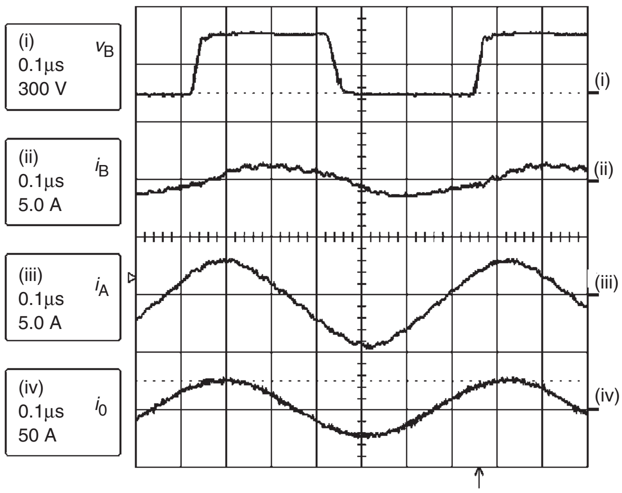

Fig. 10 *Small power throughput ($\alpha = 144^\circ$) prototype measurement*
(i) Lagging pole voltage
(ii) Lagging pole current
(iii) Leading pole current
(iv) Work piece current

for voltage-fed inverters. Figure 11 shows the converter operation when a short-circuit is applied across the work piece inductor for a control angle $\alpha = 0^\circ$ (maximum throughput). Because of the high impedance of the pole inductors, the pole current is small and assists the ZVS commutation, providing benign operating conditions for the MOSFETs.

After substituting the component values in the fundamental frequency model with those used in the prototype, the operating conditions of the inverter were compared to those obtained from the theoretical prediction. The deviations fall within 15%, and mostly occur in the region beyond $\alpha = 150^\circ$, where second-order effects unaccounted for in the model are more pronounced.

5 Conclusions

The voltage-fed LCL inverter has been shown to be able to operate at high frequency due to the use of low-voltage,

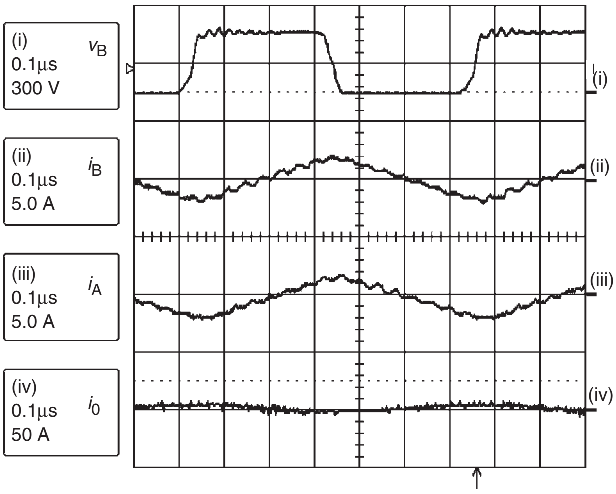

Fig. 11 *Load short-circuit operation at $\alpha = 0°$*
(i) Lagging pole voltage
(ii) Lagging pole current
(iii) Leading pole current
(iv) Work piece current

low-current MOSFETs. A further increase in operating frequency and power will enable applications such as plasma generation, dielectric heating/welding to be targeted. Due to the inverter modular structure, a larger number of poles using the same MOSFETs can be used to increase the power throughput. Load short-circuit immunity is another advantage of the inverter.

The proposed phase-shift control allows constant frequency operation and regulation down to no power throughput. This is important for operation above several megahertz where legislative restrictions on the operating frequencies apply. Operation in this frequency range necessitates ZVS, which can be provided by the proposed control.

Fundamental frequency analysis techniques have been used to analyse the inverter operation and to derive design equations. The theoretical predictions have been backed by data from time-domain simulations and measurements from a prototype.

6 References

1 Grajales, L., Sabate, J.A., Wang, K.R., Tabisz, W.A., and Lee, F.C.: 'Design of a 10 kW, 500 kHz phase-shift controlled series-resonant inverter for induction heating'. Proc. Industry applications society annual meeting, Toronto, Oat., Canada, 1993, **2**, pp. 843–849

2 Fisher, G., Doht, H.C., and Hemmer, B.: 'Operation Modes of Series Inverter 400 kHz for Induction Heating'. Conf. ERE, Proc. European power electronics, London, UK, 1993, pp. 322–327

3 Kwon, Y.-S., Yoo, S.-B., and Hyun, D.-S.: 'Half-bridge series resonant inverter for induction heating applications with load-adaptive PFM control strategy'. Proc. Applied power electronics Conf., Dalias, TX, USA, 1999, **1**, pp. 575–581

4 Dawson, F.P., and Jain, P.: 'A Comparison of Load Commutated Inverter Systems for Induction Heating and Melting Applications', *IEEE Trans. Power Electron.*, July 1991, **6**, (3), pp. 430–441

5 Kamli, M., Yamamoto, S., and Abe, M.: 'A 50-150 kHz Half-Bridge Inverter for Induction Heating Applications', *IEEE Trans. Ind. Electron.*, February 1996, **43**, (1), pp. 163–172

6 Dieckerhoff, S., Ruan, M.J., and De Doncker, R.W.: 'Design of an IGBT-based LCL-resonant inverter for high-frequency induction heating'. Proc. 34th IEEE 1999 IAS annual meeting, **3**, pp. 2039–2045

7 Sewell, H.I., Stone, D.A., and Bingham, C.M.: 'Novel, Three-Phase, Unity Power Factor Modular Induction Heater', *IEE Proc., Electr. Power Appl.*, September 2000, **147**, (5), pp. 371–378

8 Schonknecht, A., and De Doncker, R.W.: 'Novel topology for parallel connection of soft switching, high power, high frequency inverters'. Proc. 36th IEEE 2001, IAS annual meeting, Chicago, IL, USA, **3**, pp. 1477–1482

9 Federal Communications Commission, 47 CFR Chapter I, Industrial, Scientific and Medical Equipment, pp. 728–735

10 Van Loock, W.M.: 'Electromagnetic heating applications faced with EMC regulations in Europe'. Proc. Int. Symp. Electromagnetic compatibility, Tokyo, Japan, 1999, pp. 353–356

11 http://www.synopsys.com/products/mixedsignal/saber/saber.html (last accessed 17/10/2003)